Slab cracking after continuous casting of API 5L X-70 grade steel for pipeline sour gas application

R. Mendoza, J. Huante, M. Alanis, C. Gonzalez-Rivera, and J. A. Juarez-Islas

An API 5L X-70 grade steel for large diameter pipeline application with sour gas resistance was developed. The resulting Fe–C–Mn–Nb slabs were controlled rolled and accelerated cooled. In most of the slabs, mechanical properties equivalent to the above grade were broadly achieved. However, despite achieving excellent mechanical properties, during the test period, several slabs exhibited cracks in the cooling yard, causing their rejection. To elucidate the nature of the crack, several specimens were analysed by employing optical, scanning electron, and transmission electron microscopy. Microstructural characterisation together with microanalysis and thermal analysis carried out on as cast specimens showed the presence of rodlike and/or dendritelike precipitates of the Fe_2Nb type associated with the cracks. The elimination of the cracks was achieved by increasing the niobium content in the Nb ferroalloy to ensure its dissolution in the liquid bath after its addition during the alloying stage. I&S/1416

Eng. Mendoza, Eng. Huante, and Eng. Alanis are with Ispat Mexicana SA de CV, Aseguramiento de la Calidad, Fco. J. Mújica 1B, Cd. Lazaro Cardenas, Michoacan, Mexico and Dr Gonzalez-Rivera and Dr Juarez-Islas are in the Departamento de Materiales Metalicos y Ceramicos, Instituto de Investigaciones en Materiales-UNAM, Circuito Exterior S/N, Cd. Universitaria, 04510 Mexico DF, Mexico. Manuscript received 23 November 1998; accepted 15 January 1999.

INTRODUCTION

Recent developments in the Mexican pellet workshop, direct reduction, steelmaking, vacuum degassing, ladle refining/Ca treatment, and continuous casting technology have led to the production of steels containing microalloying constituents which are controlled in parts per million.[1] With regard to alloy composition, this has been a great improvement in steelmaking practice, allowing, for instance, the production of steels with low interstitial elements (C and N) and with low sulphur (to improve hydrogen induced cracking) and low phosphorus (to lower the hardening tendency of segregated regions) contents.[2] The resulting steels will have ferrite grains with very low levels of non-metallic inclusions. Sulphide shape control is also included to improve notch toughness and resistance to sour gas degradation of pipelines, leading to steels whose final microstructure and mechanical properties will depend on both steel composition and processing history.

With regard to steel chemistry, several studies have been carried out to correlate niobium contents with controlled rolling schedules plus the effect of accelerated cooling procedures, with the aim of achieving two goals, i.e. sour gas resistance and X-80 properties.[3–6] Hot rolling schedules applied to the developed X-70 steel grade were carried out to maintain a high initial temperature so that finishing roughing passes are completed at fully austenitic temperature and to ensure the dissolution of carbides, nitrides, or carbonitrides which need to be precipitated at some later stage of processing.[7] When the steel is deformed at high temperatures, recrystallisation will be complete before subsequent deformation steps. Following recrystallisation, grain growth can occur, depending on time, temperature, and amount of precipitates. As the temperature decreases, recrystallisation can be partially or totally suppressed, so that grain flattening and strain accumulation occurs.

At very low temperatures, the deformation will be extended to the austenite plus ferrite region and both phases will be deformed. Precipitate compounds will appear as the temperature of the steel decreases, supersaturating the austenite so that precipitate nucleation occurs, followed by particle growth.[8] Accelerated cooling practice after the final rolling will ensure the strength properties by controlling temperature and microstructure,[9] with the objective of forcing deformation and recrystallisation to lower temperatures and thereby maximising austenite grain refinement;[10] of course, the choice of technique used will depend on the microalloying system in use and the particular product form and manufacturing facility available.

Despite the advanced steelmaking, thermomechanical, and accelerated cooling procedure employed for the production of this kind of steel, in the trials related to this work a major problem occurred after the continuous casting of several slabs. This was related to the appearance of longitudinal cracks. The cracks ran down the length of the entire slab, perpendicular to the oscillation marks, causing rejection of the slabs. Therefore, the main aim of the present work was to identify the nature of crack initiation during the continuous casting of an API 5L X-70 grade steel for large diameter pipeline application with sour gas resistance and to propose corrective measures intended to avoid the presence of cracks in the slab.

METHODS

The steelmaking route for producing an API 5L X-70 grade steel for large diameter pipeline application with sour gas resistance consisted of charging 100% high metallisation grade sponge iron into an electric arc furnace. During the melting operation, $Ca(OH)_2$, coke, and oxygen were added. After melting and deslagging, the steel was poured from the electric arc furnace into the ladle furnace, and $Ca(OH)_2$, FeMn, and FeNi were immediately added. Then, the steel in the ladle furnace was sent to a vacuum degassing unit. During this operation, a synthetic slag was added, plus Al and CaF_2. After vacuum degassing, additions of Cu, CaF_2, FeCr, $Ca(OH)_2$, FeNb, FeSi, FeMn, and Al were carried out, always under argon stirring. After additions of ferroalloys, the 230 t of steel were continuously cast. The resulting slabs had dimensions of $0{\cdot}25 \times 1{\cdot}20 \times 6{\cdot}00$ m. Table 1 shows the final chemical composition of steels with the target mechanical properties equivalent to steel grade API 5L X-70 (after thermomechanically processing: cast 1),

together with a representative steel composition from slabs exhibiting cracks (in the as cast condition: cast 2).

In order to identify the nature of the cracks, at least 30 specimens were cut from the as cast slab in regions of the cracks. The specimens were mechanically ground using 80, 120, 240, 320, 400, 600, and 1200 emery paper, washed, mechanically polished using 1·0, 0·5, and 0·03 μm alumina, and etched in a solution of 5% nital.

For microstructure characterisation, an optical microscope, a scanning electron microscope (SEM), and a scanning transmission electron microscope (STEM) were employed, with SEM and STEM both equipped with microanalysis facilities. For the SEM observations, the specimens were ultrasonic cleaned for 20 min to remove the SiC from the grinding operation and the Al_2O_3 from the polishing operations. For the TEM observations, the thin foils were electropolished in twin jet Struers equipment by using a solution of 10% perchloric acid in ethanol at −20°C and 20 V.

Dissolution heat treatment experiments were carried out on specimens with dimensions of 0·001 m^3 that contained precipitates, and always under an argon atmosphere. A heating rate of about 78 K min^{-1} was used in the range of temperatures between 1050 and 1400°C. Once the test temperature was reached, the specimen was kept at that temperature for a period of abuot 50 min in order to ensure a uniform temperature within the specimens. Control of the test temperature was carried out by means of a Pt/Pt–18%Rd thermocouple inserted in the specimen, and the thermocouple output was plotted on a temperature register/plotter. Once the holding time was reached, the specimens were water quenched. Thermogravimetric analysis (TGA) experiments were carried out. For this purpose, $35{\cdot}4 \times 10^{-6}$ kg of a specimen containing the precipitates were placed in a platinum crucible and heated at a rate of 10 K min^{-1} under a nitrogen atmosphere in the temperature range 1050–1500°C, and the data were registered on a plotter.

RESULTS AND DISCUSSION

The main microstructure observed in the specimens far from areas of the crack was α ferrite. In the ferrite matrix the presence of carbides, TiN precipitates, precipitates in δ ferrite traces (Fig. 1*a*), and a few non-metallic inclusions of the $2CaO.6Al_2O_3$ type was observed, as shown in Fig. 1*b*. TiN precipitates and non-metallic inclusions were not associated with the crack.

In areas of the crack, rodlike and dendritelike precipitates were observed, which were confined within a group of grains, being the precipitates aligned perpendicular to the ferrite grain boundaries (Fig. 2*a*). The growth of these precipitates initiated at δ ferrite traces (Fig. 2*b*) and ended at ferrite grain boundaries, continuing to grow through the ferrite grain boundaries (Fig. 2*c*). Sometimes these rodlike precipitates adopted a dendritic morphology (Fig. 2*d*).

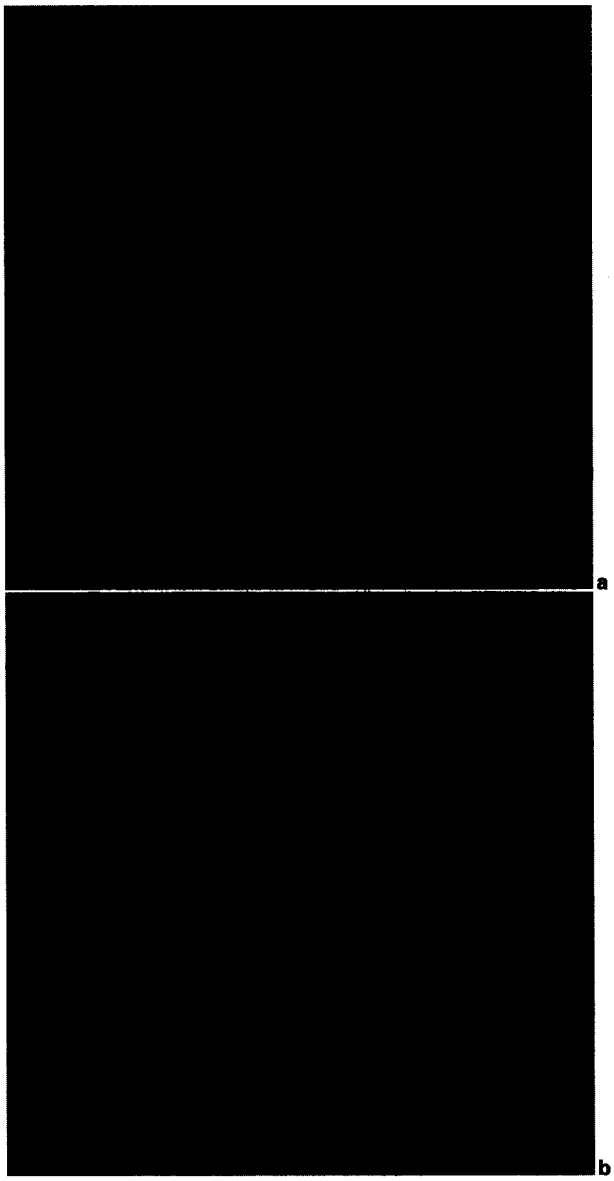

a δ ferrite traces, carbides, and TiN precipitates in α ferrite (×500); *b* non-metallic inclusions of $2CaO.6Al_2O_3$ type in α ferrite (×500)

1 Microstructure observed in specimens far from areas of crack

Table 1 Chemical composition of steel grade API 5L X-70 that satisfied its mechanical properties together with representative steel exhibiting cracks in cooling yard (in wt-%)

Element	Cast 1	Cast 2
C	0·037	0·0169
Mn	1·510	1·5500
Si	0·140	0·1470
S	0·002	0·0019
P	0·014	0·0149
Al	0·032	0·0400
Nb	0·092	0·0907
Cu	0·270	0·2740
Cr	0·266	0·2780
Ni	0·157	0·1590
Ti	0·010	0·0118
N_2	0·004	0·003
Cracks	No	Yes
YS, MPa	525·7	ND
TS, MPa	580·1	ND

ND not determined.

A representative plot of counts/s versus keV, obtained during SEM microanalyses carried out in areas where dendritelike precipitates were observed, is shown in Fig. 3*a*. According to this figure, the presence of elements such as Nb, Ti, and Mn was detected in areas where the nucleation and growth of dendrites started. When microanalyses were carried out on rodlike precipitates or dendrite arms of precipitates, elements such as Ti and Mn were not detected and only the presence of Nb was found (Fig. 3*b*). Table 2 shows SEM microanalysis results for rodlike and dendritelike precipitates. In this table it can be seen that, in areas of precipitate nucleation, elements such as Nb, Mn, and Ti were detected in a total amount of between 5·55 and 6·10 at.-%. In dendrite arms or rods, elements such as Mn and Ti were not found, and only Nb was detected in a quantity between 3·2 and 3·4 at.-%. STEM observations were carried out on thin foils containing the precipitates.

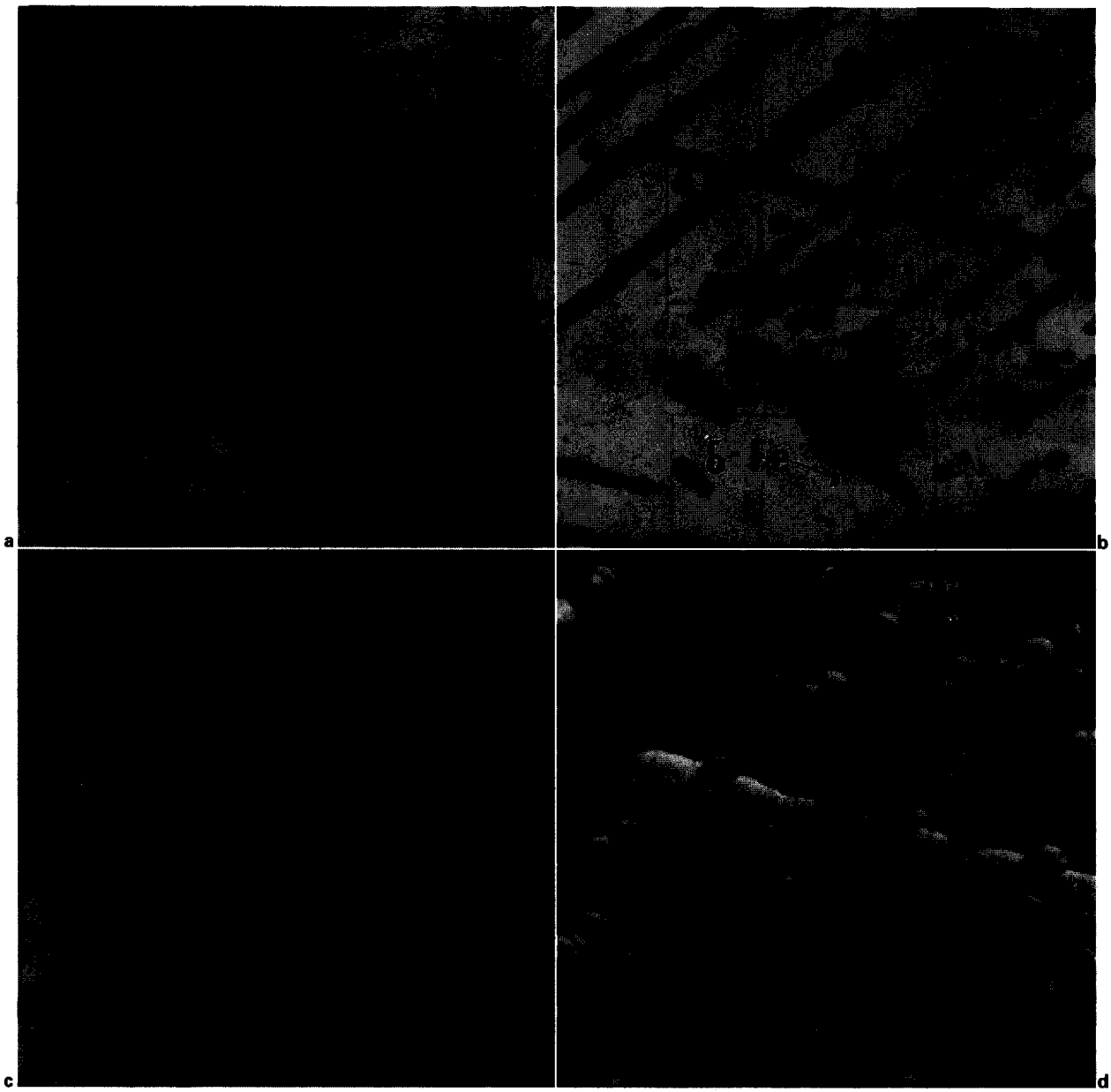

a rodlike precipitate (×125); *b* nucleation of precipitates in δ ferrite traces (×2000); *c* precipitates in matrix and grain boundaries (×1200); *d* precipitates with dendritelike morphology (×2000)

2 Microstructure observed in areas of crack

Once the precipitate was identified, as that shown in Fig. 4, microanalyses were carried out (Fig. 4*c*), detecting elements such as Fe and Nb, which were present in a range (*see* Table 3) giving a stoichiometry close to the ε Fe_2Nb compound.

Taking into account that the observed precipitates near to the crack areas were principally of an Fe–Nb nature, it was reasonable to take the Fe–Nb binary phase diagram as a reference for analysis of the problem.

Table 2 Microanalyses (SEM) carried out in areas of precipitates (in at.-%)

	Area of analysis		
Element	Nucleation of dendrite	Dendrite arms	Rods
Nb	3·30–3·50	3·2–3·4	3·2–3·4
Mn	1·50–1·73	ND	ND
Ti	0·75–0·87	ND	ND

ND not detected.

To determine the temperature range of dissolution of these precipitates, heating/cooling experiments were carried out. Figure 5 shows the plot of temperature versus time for specimens heat treated under an argon atmosphere in the temperature range 1050–1400°C with the aim of producing specimens in the γ Fe + ε, δ Fe + ε, and δ Fe + Fe_L states on the Fe–Nb phase diagram (Fig. 6).[11] Once the test temperature was reached, the specimens were kept at that temperature for ~50 min to ensure a uniform temperature within the specimens, and were then immediately water quenched. As can be seen from Fig. 5, the range of temperatures in which a total or partial dissolution of these

Table 3 Microanalyses (STEM) carried out in precipitates (in at.-%)

	Element	
Precipitate	Fe	Nb
Dendritic	65 ± 4	32 ± 6
Rod	67 ± 6	33 ± 8

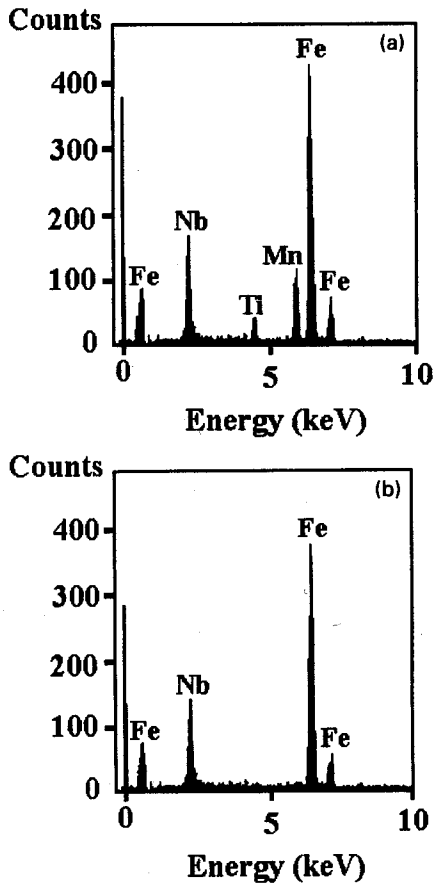

a for dendritelike precipitates; *b* for rodlike precipitates

3 Plot of counts/s versus keV

precipitates was detected was 1350–1400°C, and at temperatures <1300°C the presence of precipitates was observed. Finally, Fig. 7 shows the results of the thermogravimetric experiments, which, according to the plot of temperature difference versus temperature, indicate that at 1310°C the dissolution of Fe_2Nb precipitates started and the precipitate dissolution finished at about 1377°C. Afterwards, the transition towards δ Fe + Fe_L took place at temperatures ranging from 1377 to 1425°C.

As can be seen in Fig. 6, for the case of hypoeutectic Fe–Nb alloys the range of existence of the ε Fe_2Nb phase, formed from δ Fe boundaries, is between 3·2 at.-% (maximum solid solubility of Nb in δ Fe) and 12·1 at.-% (eutectic point). Comparing the detected amount of Nb content in areas near to the cracks with the mean Nb content in the slab (~0·09 wt-%), it was apparent that the reason behind the presence of Fe_2Nb precipitates in areas of cracks was inadequate dissolution of the FeNb ferroalloy during the alloying addition stage. Furthermore, the formation of this hypoeutectic precipitate will be enhanced with the presence of elements such as Mn and Ti, because those two elements, together with Fe, can form phases such as $NbMn_2$, $NbTi_2$, and $NbFe_2$, of the hexagonal $MnZn_2$ type.[12] The reason for the existence of these phases is that, geometrically, space may be conveniently filled by structures of the $MgCu_2$, $MgZn_2$, or $MgNi_2$ type. This implies that, during the continuous casting of the experimental steels, there is the possibility of the existence of some regions where the amount of niobium is higher than the maximum solid solubility of niobium (3·2 at.-%) in the $Fe_L + \delta$ Fe phase, giving place to the nucleation of $MgZn_2$ type precipitates when the eutectic temperature is reached.

According to the Fe–Nb phase diagram, it can be observed that, after the primary solidification of δ Fe, when the eutectic temperature (1373°C) is reached the formation

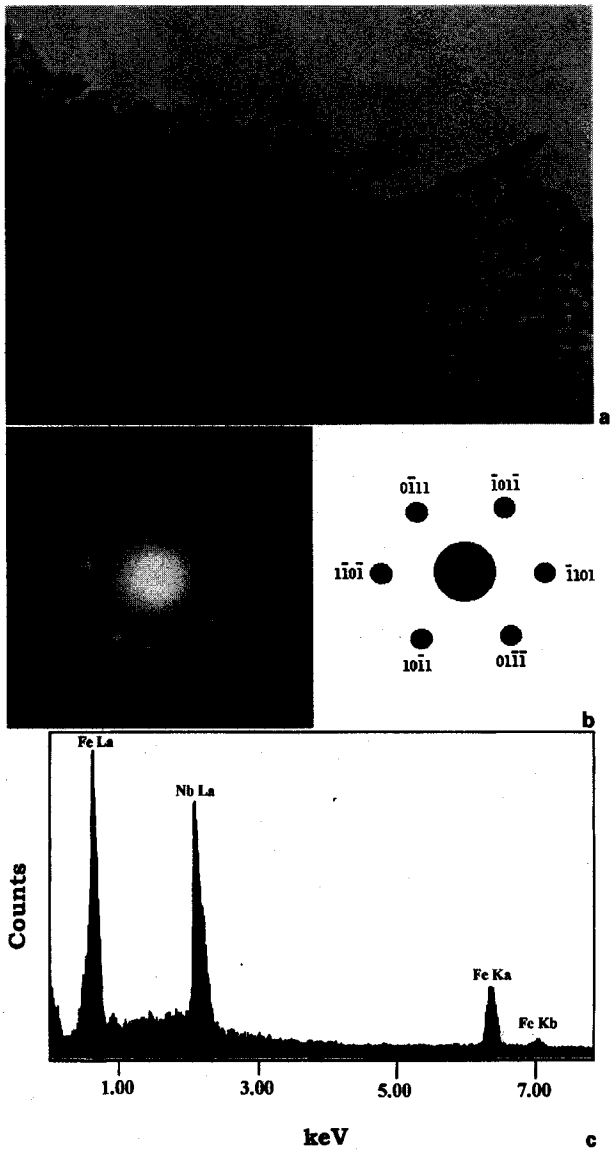

a precipitate (×30 000); *b* diffraction pattern; *c* plot of counts/s versus keV

4 Micrograph (TEM) of precipitates

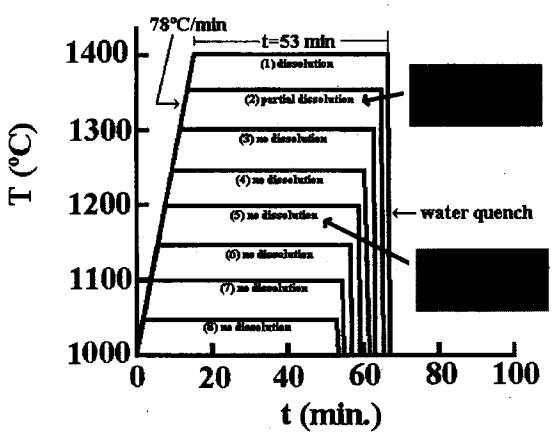

5 Plot of temperature versus time for specimens heat treated under argon atmosphere in temperature range 1050–1400°C

of ε Fe_2Nb precipitate will start in the remnant liquid, and this compound will continue to grow after the occurrence of the δ Fe→γ Fe transition.

The experimental evidence showed that Fe_2Nb precipitates are responsible for the cracking of slabs, in view of

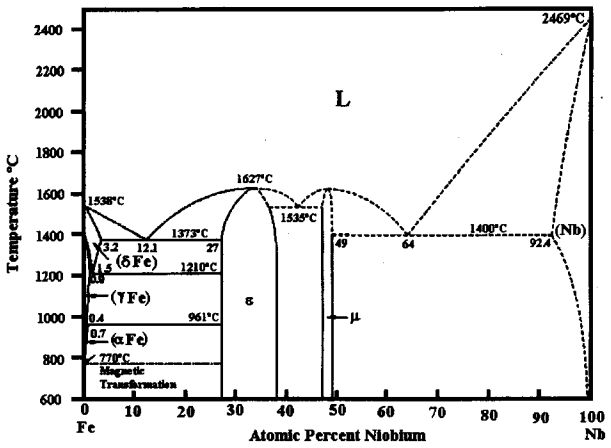

6 Fe–Nb phase diagram[11]

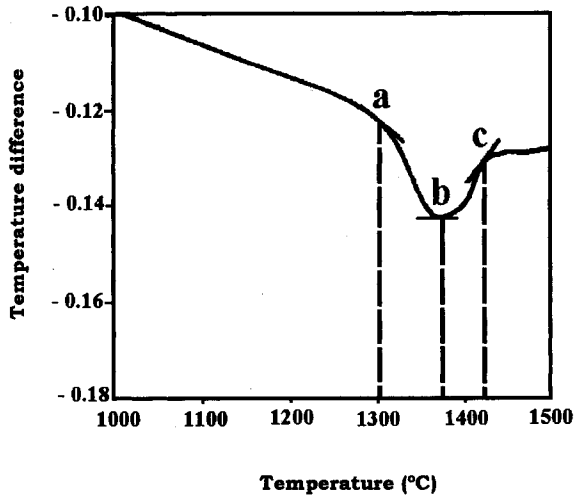

a 1310°C; *b* 1377°C; *c* 1425°C

7 Plot of temperature difference versus temperature, obtained from TGA experiments

the fact that when precipitates of this kind are not present in the slabs there is no cracking, and pointed to the measures that had to be taken in order to eliminate the slab cracking problem.

In order to avoid the formation of ε-Fe_2Nb precipitates (and cracks) in the slab, the adopted plant practice for FeNb ferroalloy addition was changed. Before, the addition was carried out after the degassing stage, at a temperature of ~1587°C of the liquid bath, which means, according to the Fe–Nb phase diagram and the Nb content (~48 at.-%) in the ferroalloy, that the temperature of the liquid bath for the dissolution of the 300 kg added to the steel needed to be ~1627°C. The new practice consisted of increasing the Nb content in the ferroalloy from 48 to 58 at.-% to decrease its melting point from 1627 to 1540°C and its weight from 300 to 270 kg and to ensure its dissolution during the stage of addition, which is just after the degassing process.

CONCLUSIONS

1. It was experimentally determined that cracks were associated with the presence of precipitates with rodlike or dendritelike morphologies.
2. These precipitates are of the Fe_2Nb type, as determined by SEM and STEM microanalysis, and their morphology will depend on the amount of Nb alone or combined with elements such as Ti and Mn.
3. Nucleation of these precipitates occurs at δ Fe grain boundaries.
4. At 1310°C the dissolution of Fe_2Nb precipitates starts and finishes at about 1377°C.
5. The new plant practice adopted for FeNb ferroalloy addition to avoid the formation of ε Fe_2Nb precipitates at δ Fe grain boundaries consisted in increasing the Nb content in the ferroalloy to decrease its melting point and to ensure its dissolution at the temperature of the liquid bath, which is 1587°C, just after the degassing stage.

REFERENCES

1. R. MENDOZA, J. CAMACHO, G. LUGO, L. HERRERA, J. REYES, C. GONZALEZ, and J. A. JUAREZ-ISLAS: *ISIJ Int.*, 1997, **37**, (2), 176–180.
2. R. MENDOZA, J. HUANTE, G. LUGO, O. ALVAREZ-FREGOSO, and J. A. JUAREZ-ISLAS: *J. Mater. Sci. Eng.* (in press).
3. K. HULKA, B. BERGMANN, and A. STREIBELBERGER: in Proc. Conf. 'Development trends in high strength structural steels', (ed. A. J. DeArdo), 177–187; Pittsburgh, PA, 1991, Iron and Steel Society.
4. K. HULKA: in Proc. Conf. 'Rolling and alloying as influencing factors on pipe steel properties, special steels and hard materials', (ed. N. R. Comins and J. B. Clarck), 267–276; 1983, Oxford, Pergamon Press.
5. T. HASHIMOTO and Y. KOMIZO: 'Development of low Pcm X70 grade line pipe for prevention of cracking during girth welding', Welding in Energy Related Project, Welding Institute of Canada, Toronto, 1983, 63–71.
6. K. HULKA, F. HEISTERKAMP, and I. I. FRANTOV: in Proc. Conf. 'An economic approach to pipe steels with high toughness and good weldability, pipeline technology', (ed. R. Denys), 43–65; 1990, Antwerp, Belgium.
7. P. E. REPAS: in Proc. Conf. 'Microalloyed HSLA Steels 88', 3–14; 1988, Chicago, IL, ASM International.
8. G. R. SPEICH, J. L. CUDDY, C. R. GORDON, and A. J. DeARDO: in Proc. Conf. on 'Phase transformations in ferrous alloys', 341–389; 1984, Warrendale, The Metallurgical Society of AIME.
9. R. S. HOSTETTER, H. KRANENBERG, and J. BATHELT: in Proc. 4th Int. Steel Rolling Conf., Deauville, France, 1987, B2.1–B2.10.
10. J. G. WILLIANS, C. R. KILLMORE, J. F. BARRET, and A. K. CHURCH: in Proc. Conf. on 'Processing, microstructure and properties of HSLA Steels'; 1988, Warrendale, Metallurgical Society of AIME.
11. 'Binary alloy phase diagrams', (ed. T. B. Massalski, J. L. Murray, L. H. Bennett, and H. Baker), Vol. 1, 1083–1084; 1987, Metals Park, OH, ASM.
12. F. LAVES and H. WITTE: *Metallwirtschaft*, 1935, **14**, 645–650.